JOURNAL OF MATERIALS SCIENCE 25 (1990) 2615–2618

Nitriding kinetics of Fe–Al–Mn–Cr–C alloys at 1000° C

JENQ-GONG DUH, CHAUR-JENG WANG
Department of Materials Science and Engineering, National Tsing Hua University, Hsinchu, Taiwan

A needle-like structure of AlN is observed in Fe–31Mn–9Al–0.87C–xCr (x = 0, 3 and 6) alloys at 1000° C in a nitrogen atmosphere. The reaction front of nitriding moves parabolically with time. The nitriding rate is evaluated on the basis of the penetration depth of the nitriding layer at various lengths of time, and is found to be increased with increasing chromium content in the alloy. A quasi-steady state diffusion model is employed to investigate the nitriding kinetics by nitrogen migration through the alloy matrix. The nitriding rate depends on the solubility of nitrogen as well as the diffusivity of nitrogen in the alloy system. It is argued that the solubility of nitrogen predominates the nitriding, and thus the growth of AlN prevails in the austenitic phase instead of ferrite, due to the higher nitrogen solubility in austenite. In addition, the chromium alloying into the Fe–Al–Mn system increases the lattice parameter, which leads to a higher solubility of nitrogen, and hence a higher nitriding rate is obtained.

1. Introduction

Over the past years, a great deal of research activity has focused on the development of the potential Fe–Al–Mn–based alloy as a substitute for conventional Fe–Ni–Cr stainless steel. The high-temperature oxidation behaviour of this alloy system has been intensively investigated [1–12]. A series of work has been carried out continuously in our research group concerning the high-temperature behaviour of Fe–Al–Mn based alloys, including the elemental distribution and formation morphology in the oxidation layer [7, 9, 11], the effect of gaseous atmosphere and pretreatment [10], the development of the oxidation-induced ferrite layer [12], and the proposed diffusion-related mechanism in the oxidation-induced phase transformation [13]. Recently, a nitriding phenomenon was observed in Fe–31Mn–9Al–6Cr–0.86C alloy oxidized in dry air at temperatures above 800° C [14]. A needle-like nitriding product of AlN developed towards the alloy matrix. It was argued that the degree of solubility of nitrogen played a major role in the nitriding. The austenitic phase with higher nitrogen solubility was observed to promote the growth of AlN, while the ferrite phase exhibited the reverse effect. The purpose of the present study was to investigate the kinetics of the nitriding behaviour. The thickness of the nitriding layer is measured as a function of the oxidation time and employed to evaluate the nitriding rate of the Fe–Al–Mn alloy. The nitriding kinetics is discussed with respect to the nitrogen solubility as well as the diffusivity of the constituent.

2. Experimental techniques

The alloy was prepared by vacuum induction melting from high-purity elements. The chemical composition is given in Table I as obtained by the wet chemical method. The as-fabricated ingots were forged at 1200° C with 75% reduction and then homogenized at 1200° C for 11 h. After surface finishing, the alloys were then rolled with 90% reduction to 2.3 mm thickness. The details of the alloy fabrication and sample preparation were reported elsewhere [10, 11, 14].

The specimen was first put into a specially designed stainless steel (AISI-310) tubing, and followed by outgassing with nitrogen purging. The outgassed tubing was then placed within the constant-temperature zone in a tube furnace. The nitriding experiment was carried out at 1000° C in a flowing nitrogen (99.995%) atmosphere for times ranging from 1 to 24 h. The morphologies of the nitriding layer were examined by optical and scanning electron microscopy.

3. Results and discussion

3.1. Morphology and penetration depth of the nitriding layer

Fig. 1 shows the optical micrograph of alloy C nitrided at 1000° C for 24 h, which is a typical morphology of the nitriding layer among alloys A, B and C. A region containing needle-like structure is observed beneath the free surface. The nitriding takes place mainly in the austenitic phase due to the higher solubility of nitrogen [14]. The needle-like structure is

TABLE I Chemical compositions (wt %) of the alloys employed in this study

Alloy	Mn	Al	Cr	C	Fe
A	31.18	8.69	–	0.87	Bal.
B	31.30	8.92	5.96	0.86	Bal.
C	30.95	8.87	2.98	0.87	Bal.

0022–2461/90 $03.00 + .12

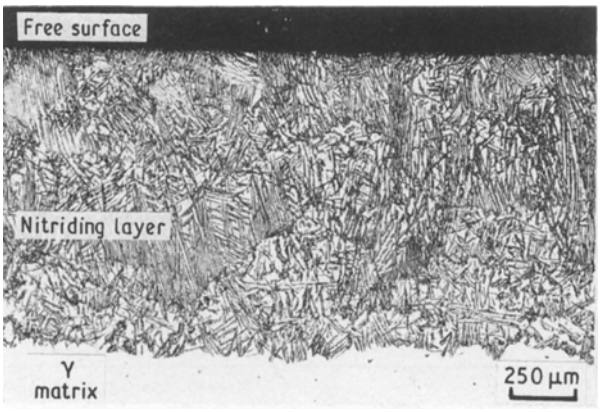

Figure 1 Optical micrograph of alloy C nitridized in pure nitrogen at 1000° C for 24 h.

identified as AlN, and the nitriding behaviour is fairly sensitive to the alloy surface condition [10].

Table II lists the penetration depths of the nitriding layer for alloys A, B and C. The corresponding plot of thickness of the nitriding layer against the square root of time is represented in Figs 2 to 4 for alloys A, B and C, respectively. It is apparent that the nitriding layer grows parabolically with time. According to the parabolic rate law formulation

$$\xi = (K_N t)^{1/2} \quad (1)$$

where ξ is the thickness of the nitriding layer, K_N is the nitriding rate, and t is the nitriding time. The nitriding rates, K_N, for various alloys at 1000° C are evaluated and are given in Table III. It appears that the nitriding rate increases with the chromium content. The effect of chromium content on the nitriding behaviour will be discussed later.

For alloys oxidized in air, three distinct layers were observed [10]. The outer layer is identified as $(Fe, Mn)_3O_4$. Mixed phases of AlN, MnO and $Fe(Al, Cr)_2O_4$ are found in the middle layer; while a region containing needle-like structure AlN is observed in the inner layer. It appears that the nitriding is ahead of the oxidation for the alloy oxidized in air. As nitriding occurs prior to oxidation and results in AlN, the content of aluminium is depleted between the needle-like structure. A quantitative analysis with the aid of electron microprobe (Jeol JCXA-733) indicates that the aluminium content between the AlN plates is only 0.08 wt %.

3.2. Nitriding kinetics

In the austenitic structure of Fe–Al–Mn–Cr–C alloy, nitrogen would be located in the interstitial site, while aluminium is in the substitutional lattice. Relatively speaking, the diffusivity of nitrogen, D_N, is greater than that of aluminium, D_{Al}, i.e.

$$D_N \gg D_{Al} \quad (2)$$

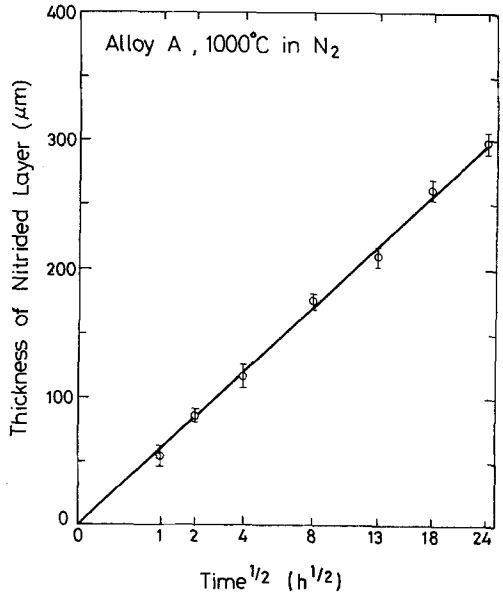

Figure 2 The penetration depth of the nitrided layer as a function of time for alloy A at 1000° C.

Grabke *et al.* [15] reported the solubility of nitrogen for Fe–28.6 at % Mn alloy at 1000° C in 0.95 atm N_2 to be around 1.49 at %. The aluminium content in the matrix is 16.4 at % for alloy C in this study. Thus there is more than one order of magnitude difference between the nitrogen solubility, $N_N^{(s)}$, and the initial concentration of aluminium, $N_{Al}^{(0)}$. If effects from other alloying elements are neglected, one has

$$N_N^{(s)}/N_{Al}^{(0)} \ll 1 \quad (3)$$

With conditions described by Equations 2 and 3, the nitriding behaviour in Fe–Al–Mn–base alloy can be considered to be another type of internal oxidation according to Wagner's formulation [16]. The internal nitriding migrates through the inward diffusion of nitrogen, and aluminium in the internal matrix is presumed to be nitrided immediately on the spot. The rate of nitriding can be derived for a planar specimen geometry by the quasi-steady state approximation. Consider a planar specimen of a multicomponent alloy A–B–C in which A forms a very stable nitride. Assume the ambient P_{N_2} is too low to nitride elements B and C but high enough to nitride element A. A schematic concentration for the internal nitriding is shown in Fig. 5.

The quasi-steady state approximation assumes the dissolved nitrogen concentration varies linearly across the zone of internal nitriding [17]. The nitrogen flux, J, through the internal nitrided zone is given by Fick's first law as

$$J = D_N \frac{N_N^{(s)}}{\xi V_m} \quad (4)$$

TABLE II The penetration depth (μm) of nitriding layer at 1000° C for the alloys employed in this study

Alloy	Time (h)						
	1	2	4	8	13	18	24
A	54.7 ± 16.8	86.2 ± 10.4	116.9 ± 18.9	175.5 ± 12.1	209.4 ± 15.9	261.8 ± 16.5	298.9 ± 17.6
B	68.4 ± 12.4	109.6 ± 21.3	156.4 ± 18.1	219.8 ± 13.5	275.9 ± 25.3	326.8 ± 15.3	377.8 ± 22.7
C	100.1 ± 12.5	146.6 ± 18.7	188.9 ± 19.5	284.1 ± 19.5	365.2 ± 16.8	428.3 ± 19.6	498.5 ± 28.2

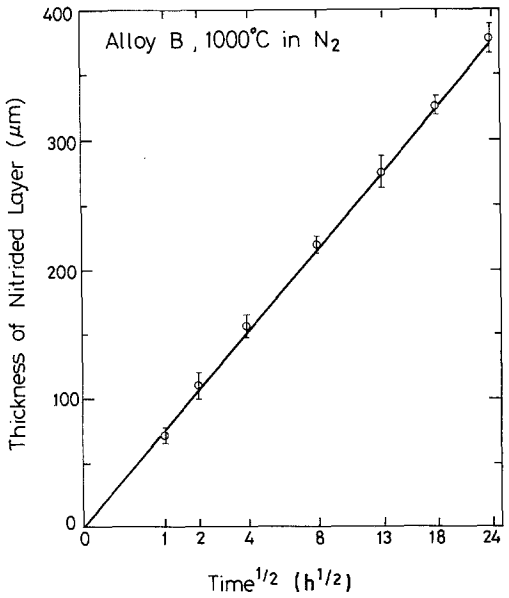

Figure 3 The penetration depth of the nitrided layer as a function of time for alloy B at 1000° C.

where $N_N^{(s)}$ is the nitrogen solubility in element A, V_m is the molar volume of the matrix alloy, D_N is the diffusivity of nitrogen in the alloy, and ξ is the penetration depth of the nitridized layer.

Alternatively, the amount of nitrogen accumulated in the internal nitrided zone per unit area of the reaction front is

$$m = \frac{N_A^{(0)} v \xi}{V_m} \tag{5}$$

where $N_A^{(0)}$ is the initial solute concentration in the matrix, and v is the stoichiometric ratio in compound AN_v.

Differentiation of Equation 5 with respect to time gives another expression for the flux

$$J = \frac{dm}{at} = \frac{N_A^{(0)} v}{V_m} \frac{d\xi}{dt} \tag{6}$$

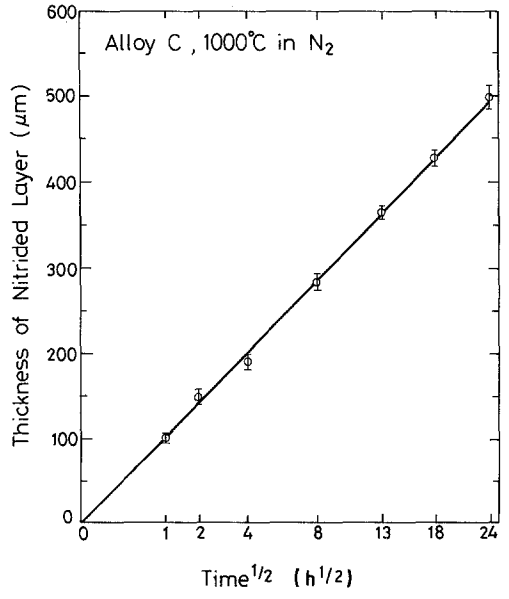

Figure 4 The penetration depth of the nitrided layer as the function of time for alloy C at 1000° C.

TABLE III The calculated nitriding rate for the alloys at 1000° C

Alloy	Nitriding rate (10^{-8} cm^2 sec^{-1})
A	1.06 ± 0.05
B	1.69 ± 0.04
C	2.90 ± 0.09

Equating Equations 4 and 6, rearranging and integration from $\xi = 0$ at $t = 0$ to the point of interest at time, t, for the penetration depth, ξ, one obtains

$$\xi = \left[\frac{2N_N^{(s)} D_N}{vN_A^{(0)}} t\right]^{\frac{1}{2}} \tag{7}$$

In the case of Fe–Al–Mn-base alloy, $v = 1$ for compound AlN, $N_A^{(0)} = N_{Al}^{(0)} = 0.164$ in alloy C, thus

$$\xi = [12.2\, N_N^{(s)} D_N t]^{\frac{1}{2}} \tag{8}$$

Comparing Equation 8 with Equation 1

$$K_N = 12.2 N_N^{(s)} D_N \tag{9}$$

Equation 9 implies that the nitriding rate is dependent on the diffusivity of nitrogen, as well as the solubility of nitrogen. In principle, Equation 9 provides the evaluation of nitrogen diffusivity if the solubility of nitrogen is known. Unfortunately, no nitrogen solubility data are available in the literature for Fe–Al–Mn-base alloy. A preliminary study has been conducted to measure the nitrogen content through X-ray microanalysis with an electron microprobe (Jeol JCXA-733). However, at most the interspacing between AlN is smaller than 1 μm, which makes the data less reliable, as 1 μm is somewhat smaller than the excitation volume of the electron beam in the specimen. Nevertheless, an approximate nitrogen diffusion coefficient can be obtained if one adopts the solubility of nitrogen in Fe–Mn alloy given by Grabke *et al.* [15]. Substituting $N_N^{(s)} = 0.014$ into Equation 8, a magnitude of $D_N = 10^{-7}$ cm^2 sec^{-1} is obtained in this Fe–Al–Mn-base alloy. It should be pointed out that $D_N = 10^{-7}$ cm^2 sec^{-1} has a similar order of magnitude compared to the case of nitriding in Cr–Ti alloy [18]. The nitriding rate in the Cr–Ti system is, however, two orders of magnitude smaller than that in the Fe–Al–Mn system. This might imply that the solubility of nitrogen, instead of the diffusivity of nitrogen, predominates the nitriding phenomena in a multicomponent system.

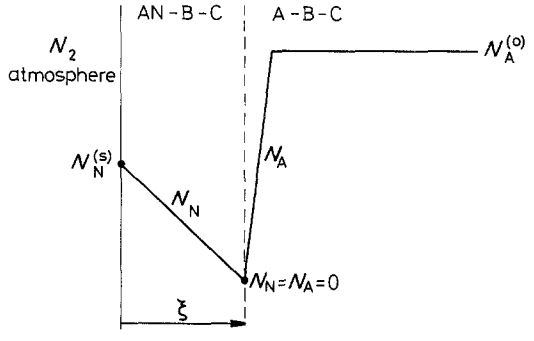

Figure 5 Schematical concentration profiles for the internal nitriding of a multicomponent alloy A–B–C.

TABLE IV Lattice parameters and densities for the alloys employed in this study

Alloy	Structure	Lattice parameter (nm)	Density ($g\,cm^{-3}$)
A	γ	0.36822 ± 0.00191	6.8698
B	γ	0.36886 ± 0.00165	6.7645
C	γ	0.36912 ± 0.00240	6.7615

In fact, the solubility of the solute element depends upon the phase of microstructure in the alloy system. Generally speaking, the solubility of nitrogen in the ferrite phase is smaller than that in the austenitic phase. Thus the growth of AlN prevails in the austenitic region instead of the ferrite, which is consistent with the previous observation [14].

3.3. The effect of chromium alloying

It is observed that the nitriding rate in this study increases as the chromium content increases, as shown in Table III. At 1000° C, alloys A, B and C all exhibit austenitic structure. Nitrogen is presumed to be located in the interstitial site, and no significant change is predicted with the addition of chromium. Grabke *et al.* [15] proposed that the chromium addition in the Fe–Mn system would increase the solubility of nitrogen in the alloy. Because the atomic sizes of chromium and manganese are larger than that of iron, the addition of chromium enlarges the lattice parameter and consequently increases the interstitial site spacing, which in turn enhances the nitrogen content in the interstitialcy. Table IV gives the lattice parameters and densities for alloys A, B and C in this study. It is apparent that the lattice parameter increases with the increasing chromium content. Hence the nitriding rate is enhanced for the alloy with a greater chromium content.

4. Conclusions

1. Alloys with compositions Fe–31Mn–9Al–0.87C–xCr (x = 0, 3 and 6) develop a needle-like nitriding product of AlN in a nitrogen atomsphere at 1000° C.

2. The reaction front of the nitriding layer migrates parabolically with time. The measured penetration depth and the evaluated nitriding rate increases with the chromium content in the alloy.

3. The kinetics of nitriding is presented with a quasi-steady state diffusion model of nitrogen migration through the alloy. The nitriding rate depends on the solubility of nitrogen and the diffusivity of nitrogen in the alloy system.

4. The solubility of nitrogen is considered to be the dominating factor in the nitriding behaviour. The growth of AlN prevails in the austenitic phase instead of ferrite due to the higher nitrogen solubility in the austenite.

5. Addition of chromium into Fe–Al–Mn alloy increases the lattice parameter and enhances the solubility of nitrogen which results in a higher nitriding rate.

Acknowledgement

The authors thank the National Science Council, Taiwan, for financial support under contract no. NSC–78–0405–E007–12.

References

1. S. K. BANERJI, in "Workshop on Trends in Critical Materials Requirements for Steels of the Future-Conservation and Substitution Technology for Chromium", Vanderbilt University, Nashville, Tennessee, October, 1982.
2. J. P. SAUER, R. A. RAPP and J. P. HIRTH, *Oxid. Met.* **18** (1982) 285.
3. P. TOMASZEWICZ and G. R. WALLWORK, *ibid.* **20** (1983) 75.
4. P. R. S. JACKSON and G. R. WALLWORK, *ibid.* **21** (1984) 135.
5. *Idem, ibid.* **20** (1983) 1.
6. R. WANG, M. J. STRASZHEIM and R. A. RAPP, *ibid.* **21** (1984) 71.
7. J. G. DUH, C. J. LIN, J. W. LEE and C. M. WAN, in "Proceedings of Alternate Alloying for Environmental Resistance", edited by G. R. Smolik and S. K. Banerji (The Metallurgical Society, Warrendale, Pennsylvania, 1987) p. 283.
8. C. H. KAO, C. M. WAN and M. J. JAHN, *ibid.* p. 347.
9. J. G. DUH, C. J. WANG, C. M. WAN and B. S. CHIOU, *ibid.* p. 291.
10. C. J. WANG and J. G. DUH, *J. Mater. Sci.* **23** (1988) 2913.
11. *Idem, ibid.* **23** (1988) 3447.
12. J. G. DUH, J. W. LEE and C. J. WANG, *ibid.* **23** (1988) 2649.
13. J. G. DUH and J. W. LEE, *J. Electrochem. Soc.* **136** (1989) 847.
14. C. J. WANG and J. G. DUH, *J. Mater. Sci.* **23** (1988) 769.
15. H. J. GRABKE, S. K. IYER and S. K. SRINIVASAN, *Z. Metallkde* **66** (1975) 286.
16. C. WAGNER, *J. Electrochem. Soc.* **63** (1959) 777.
17. N. BIRKS and G. H. MEIER, in "Introduction to High Temperature Oxidation of Metals" (Edward Arnold, London, 1983) p. 95.
18. J. L. ARNOLD and W. C. HAGEL, *Met. Trans.* **3** (1972) 1471.

Received 23 January
and accepted 24 August 1989